International Journal of Machine Learning and Cybernetics (2025) 16:1111–1127
https://doi.org/10.1007/s13042-024-02325-x

ORIGINAL ARTICLE

A data-driven mixed integer programming approach for joint chance-constrained optimal power flow under uncertainty

James Ciyu Qin[1] · Rujun Jiang[2] · Huadong Mo[1] · Daoyi Dong[1,3]

Received: 14 September 2023 / Accepted: 11 August 2024 / Published online: 31 August 2024

Abstract

This paper introduces a novel mixed integer programming (MIP) reformulation for the joint chance-constrained optimal power flow problem under uncertain load and renewable energy generation. Unlike traditional models, our approach incorporates a comprehensive evaluation of system-wide risk without decomposing joint chance constraints into individual constraints, thus preventing overly conservative solutions and ensuring robust system security. A significant innovation in our method is the use of historical data to form a sample average approximation that directly informs the MIP model, bypassing the need for distributional assumptions to enhance solution robustness. Additionally, we implement a model improvement strategy to reduce the computational burden, making our method more scalable for large-scale power systems. Our approach is validated against benchmark systems, i.e., IEEE 14-, 57- and 118-bus systems, demonstrating superior performance in terms of cost-efficiency and robustness, with lower computational demand compared to existing methods.

Keywords Chance-constrained optimisation · Mixed integer programming · Optimal power flow

List of symbols

$\mathcal{P}$	Ambiguity set
$\mathcal{U}$	Uncertainty set
β_i	Participation factor of the ith generator
ϵ	Violation probability
$\mathcal{B}$	Set of buses
$\mathcal{G}$	Set of conventional generators
$\mathcal{L}$	Set of transmission branches
Ω	Total power mismatch
ω_i	Fluctuation at the ith bus
Φ	Power transmission distribution factor
d_i	Forecast load at the ith bus
f_{ij}	Power flow on line ij
f_{ij}^{LB}	Lower bound of f_{ij}
f_{ij}^{UB}	Upper bound of f_{ij}
g_i	Scheduled power generation
M	Big-M coefficient
N	Number of scenarios

Abbreviations

AC	Alternating current
AGC	Automatic generation control
CCs	Chance constraints
DC	Direct current
DRO	Distributionally robust optimization
GP	Gaussian process
GPR	Gaussian process regression
JCC	Joint chance-constrained
MIP	Mixed integer programming
PTDF	Power transmission distribution factor
OPF	Optimal power flow
RC	Robust constraints
RO	Robust optimization
SA	Scenario approach
SAA	Sample average approximation
SCC	Single chance-constrained

✉ Huadong Mo
huadong.mo@unsw.edu.au

James Ciyu Qin
ciyu.qin@unsw.edu.au

Rujun Jiang
rjjiang@fudan.edu.cn

Daoyi Dong
daoyi.dong@anu.edu.au

[1] School of Engineering and Technology, University of New South Wales, Northcott Drive, Canberra, ACT 2612, Australia

[2] School of Data Science, Fudan University, Handan Road, Yangpu District, Shanghai 20043, China

[3] CIICADA Lab, School of Engineering, Australian National University, University Avenue, Canberra, ACT 2601, Australia

SDP Semidefinite programming
SOC Second-order cone

1 Background

In power systems, power balance is performed continually. Optimal power flow (OPF) is a power dispatching mechanism that performs every 5–30 min in a power system for generators to provide sufficient energy with the lowest operational costs while maintaining system reliability and security [1]. The traditional OPF model considers only the limitations of physical components in the system, i.e., the power balance, constraints of generation plants and power flows. Such a problem can be easily formulated and solved deterministically, and power generation can be scheduled accordingly to satisfy the forecast load. While the involvement of renewable generation has brought additional uncertainties, limits for the physical components are more likely to be reached. Therefore, studies of OPF considering uncertainties were conducted to incorporate fluctuations in renewable energy.

2 Literature review

2.1 Uncertainty modeling techniques

Modeling uncertainties in power systems is pivotal for ensuring reliability and efficiency. The integration of uncertainties, whether from stochastic load, renewable generation, or other sources, significantly affects operational costs and causes the system to violate constraints. Techniques like probabilistic models, stochastic optimization, and robust optimisation manage unpredictability inherent in system variables like load demand and generation capacity. A common approach in alternating current (AC) and direct current (DC) OPF models is chance-constrained programming, defining a risk parameter for constraint violation.

Recent literature showcases diverse uncertainty modeling approaches. A study [2] in automatic generation control (AGC) systems under non-Gaussian wind power uncertainty employed an Ito-theory-based model with a stochastic control approach for computational efficiency. This method transforms the stochastic control problem into a deterministic one, maintaining performance while reducing computational complexity. The study in [3] explored uncertainty quantification in power system dynamics through polynomial chaos-based methods. A generalized polynomial chaos model offers computational efficiency for short-term simulations, while a multi-event generalized polynomial model provides enhanced accuracy and stability for long-term scenarios, both effectively handling diverse uncertainty distributions. Another work [4] presented an uncertainty evaluation algorithm for power systems with correlated renewable sources using the probabilistic collocation method and Copula function. This approach efficiently models nonparametric distributions using kernel density estimation, offering improved accuracy and reduced computational load in quantifying system stability uncertainties. In social event detection, Ren et al. [5] presented an uncertainty-guided contrastive learning loss framework for imbalanced social event detection, leveraging evidential deep learning and Dempster–Shafer theory for uncertainty estimation. This approach emphasizes boundary learning in latent space, dynamically adjusting class separability based on uncertainty, thereby improving the detection of uncertain classes.

These diverse methodologies underscore the importance of context-specific approaches to uncertainty modeling in various domains. In our ongoing research, we are exploring the application of chance-constrained programming in AC and DC OPF models. This approach, aligning with the trends observed in current literature, aims to offer a flexible and realistic framework for addressing uncertainties in power generation and demand, contributing to the broader discourse on effective uncertainty management in power systems.

2.2 AC and DC-OPF

To account for the uncertainties in a power system, introducing chance constraints (CCs) into the OPF problem is a common approach. These CCs can define a risk parameter to allow constraint violation, which is crucial in both AC and DC-OPF models.

Chance-constrained AC-OPF [6–14] accounts for voltage magnitudes, active, and reactive power, but faces challenges due to the nonlinearities of the power flow equations and the CCs. These nonlinearities often necessitate linearization steps for computation. For example, Zhang and Li [6] modeled the OPF problem with chance-constrained programming under uncertain loads, applying linearization to establish a relationship between constrained outputs and uncertain inputs. Similar linearization strategies were adopted by [8, 9], with the latter focusing on voltage magnitude control but requiring further investigation into scalability.

The nonlinear nature of AC-OPF introduces nonconvexities, often resulting in a feasible space with multiple disconnected components [15]. This complexity has led to many optimisation problems within AC power flow systems being classified as NP-Hard [16, 17]. While metaheuristic algorithms, such as whale optimisation [18], reptile search [19], and partial swarm optimisation [20], exist to ensure global optimal, they often do not provide explicit solutions and are very time-consuming, especially when uncertainties

are integrated into the system. This integration becomes critical in short-term planning, where uncertainties from stochastic load and renewable generations have significant impacts on operational costs and constraints [21]. Recent advancements, like deep reinforcement learning approaches such as proximal policy optimisation, have shown promise in managing distribution networks with renewable energy and storage devices [22, 23]. However, they too face difficulties in providing explicit solutions in a computation-efficient manner under uncertainty. Therefore, distributed computing methods have been proposed to improve computational efficiency [24, 25], including solving the OPF problem while preserving confidentiality [25]. Nonetheless, probabilistic AC power flow models might produce multiple or no solutions, posing significant challenges in assessing the impact of uncertainties.

In contrast, the DC-OPF model, being a linear approximation, simplifies the integration of uncertainties. This model has seen extensive exploration in applying different chance-constrained optimisation techniques [26–39]. Approaches range from assuming distributions for uncertain variables to adopting distributionally-robust methods and sample-based approaches that do not require distributional assumptions or ambiguity sets. Such techniques in DC-OPF provide a reference for power system operators, with the potential for achieving reasonable solutions within a feasible timeframe.

2.3 Joint chance constraints

The majority of chance-constrained OPF problems in the current literature are predominantly solved using a single chance constraint approach. Despite its prevalence, this method often fails to capture complex interdependencies between multiple system components, which can be crucial for the overall system reliability. Recognising this limitation, some researchers have explored joint chance-constrained (JCC) formulations, which ensure that all engineering limits are met concurrently with a joint probability, thus offering a more robust guarantee of system security [40].

The single chance constrained (SCC) OPF, while simpler to solve due to its focus on individual constraints with unique probabilities [41], can result in solutions that exhibit a lower overall joint violation probability [34]. This existing outcome suggests that while SCC OPF is computationally efficient, it might not always provide the most reliable or cost-effective solutions.

Conversely, the JCC approach requires multiple constraints to be satisfied simultaneously with a prescribed probability, emphasising a holistic view of system security. This approach, however, presents significant computational challenges. A common strategy is to decompose the JCC problem into a series of single CCs, as demonstrated in [13], which simplifies the problem but requires careful allocation of individual risk levels. Selecting these risk levels optimally is crucial for accurately approximating the JCC problem [42], yet it often leads to overly conservative and costly solutions [35, 43].

In this paper, we address the complexities of JCC optimisation by proposing a model that employs the JCC framework comprehensively. We evaluate the risk across the entire system collectively, rather than assessing individual constraints separately. This holistic consideration of system-wide risk enables a more accurate and unified assessment of uncertainties. By solving all constraints concurrently without decomposing them into simpler components, our model avoids producing overly conservative solutions that typically incur higher costs. This direct and integrated approach ensures robust system security while optimising computational efficiency. This approach aims to strike a balance between the ease of solution and the assurance of overall system security.

2.4 Reformulations of chance constraints

CCs are inherently nonlinear and nonconvex, making them challenging to compute and solve deterministically; thus, reformulations are often necessary. The work [10] introduced a convex relaxation of the chance-constrained DC OPF using a semidefinite programming (SDP) reformulation, incorporating both Gaussian distributed uncertainties and realistic forecast data. They demonstrated that realistic data could yield solutions with reduced computation time and violation probability. The work [26] proposed a second-order cone (SOC) reformulation of the probabilistic constrained OPF, targeting minimum generation costs while accommodating random power injections, thereby enhancing computational tractability. Through extending the results in [26, 34] developed a corrective control policy based on normally distributed forecast uncertainties, reformulating the CC OPF problem as an SOC program efficiently solvable for large systems. Several authors in [34] further advanced this approach in [8], constructing an AC model that uses partial linearisation for nonlinear CCs, reducing computation time through an iterative algorithm. In [29], the authors assumed a multivariate normal distribution of uncertainties, devising an analytical reformulation using confidence bound approximations, which could be effectively addressed with a cutting-plane algorithm.

Building upon [26, 32] adopted a robust optimisation framework, considering uncertainty sets for the mean and variance of Gaussian distributions. Although this method employed a cutting-plane algorithm, it sometimes failed to maintain high reliability, especially under JCC. Distributionally robust optimisation (DRO) has gained traction, as exemplified by [11, 30, 31], where the authors formulated ambiguity sets based on empirical data moments. These

approaches, despite being more reliable, often result in longer computation time. The work [31] addressed two-sided CCs with DRO, facilitating efficient solutions through standard solvers. Conversely, Xu et al. [44] critiqued the reliance on mean and variance alone, pointing out the impracticality of ignoring tail events in distributions, which are crucial given that constraint violations typically occur in these regions.

In summary, while direct analytical reformulations of CC often rely on assumptions about uncertainty distributions, they generally overlook tail events, as [10] suggested. Utilizing realistic scenarios for deriving optimal solutions can be more practical. The sample average approximation (SAA) method leverages realistic scenarios without presuming an uncertainty set, using an empirical distribution to approximate CCs [47]. This approach enables direct problem-solving via mixed integer programming (MIP), which, unlike the method used by [28], does not impose stringent data size requirements due to its direct modelling of constraint violations using binary variables. In summary, Table 1 presents the comparison between recent work and ours in terms of test system, type of CCs, types of CCs reformulation and uncertainty representation.

2.5 Contributions

The contributions of this paper are summarised as follows.

1. We introduce a novel SAA method applied to JCC OPF models considering uncertain load and renewable energy generation. This approach enhances the traceability of the problem without compromising the solution quality, offering a practical solution framework that bridges the gap between theoretical robustness and operational feasibility.
2. Unlike existing approaches that rely on distributional assumptions of uncertainties, our method leverages historical data to formulate an MIP that can be directly solved with off-the-shelf solvers. This strategy significantly mitigates the risks associated with distributional assumptions and inaccuracies, providing a more reliable basis for decision-making in uncertain environments.

Table 1 The comparison between recent work and the proposed work

References	Year	Test system	Type of CCs	Type of CCs reformulation	Uncertainty representation
[40]	2013	IEEE 30-bus system	Single	Convex reformulation, Heuristic algorithm	Scenarios, quantiles
[45]	2017	IEEE 118-, 300-bus systems	Joint	Analytical reformulation	Distribution, moments
[46]	2018	RTS96, IEEE 118-, 300-bus systems, Polish 2383 system	Joint	Analytical reformulation	Distribution
[9]	2017	IEEE 37-bus system	Single	Convex reformulation	Distribution
[10]	2018	IEEE 24-, 118-bus systems	Joint	Semidefinite reformulation	Uncertainty set
[11]	2018	IEEE 14-, 118-bus systems	Single	Distributionally robust reformulation	Family of probability distributions
[12]	2019	IEEE 5-, 30-bus systems	Single	Moment-based reformulation	Moments
[13]	2019	IEEE 37-bus system	Joint	Analytical reformulation	Scenarios
[14]	2019	IEEE 118-bus system	Joint	Analytical reformulation	Distribution
[26]	2014	IEEE 9-, 30-, 39-, 118-bus systems	Single	Conic reformulation	Distribution, moments
[28, 29]	2017	IEEE 30-bus system	Single	Analytical reformulation	Distribution
[30]	2016	IEEE 3-, 39-, 118-bus systems	Single	Distributionally robust reformulation	Family of probability distributions
[31]	2017	IEEE 39-bus system	Joint	Distributionally robust reformulation	Family of probability distributions
[32]	2015	BPA system	Single	distributionally robust reformulation	Family of probability distributions
[33]	2020	IEEE 5-, 118-bus systems	Single	Distributionally robust reformulation	Family of probability distributions
[35]	2020	IEEE 14-, 57-, 118-bus systems	Joint	Sample-based approximation	Scenarios
[36]	2021	IEEE 5-, 118-bus systems	Single	Analytical reformulation	Distribution, scenarios
[37]	2021	IEEE 9-, 14-, 30-, 118-, 300-bus systems	Joint	Distributionally robustreformulation	Family of probability distributions
[38]	2020	IEEE 118-bus system	Joint	Boolean Reformulation	Scenarios
Our work	–	IEEE 14-, 57-, 118-bus systems	Joint	Data-driven MIP reformulation	Scenarios

3. Our model addresses the joint chance constraints in their entirety, avoiding the common practice of decomposing them into individual constraints. This holistic view prevents the suboptimal and overly conservative solutions often associated with individual constraint optimisation. By considering all constraints jointly, our approach ensures a more accurate representation of system-wide risk levels and operational reliability.
4. To tackle the challenge of increasing complexity with larger sample sizes in MIP, we implement a model improvement strategy that significantly reduces the number of binary variables required. This adjustment lowers the computational burden, making our method more practical and scalable compared to existing approaches, which often struggle with computational intractability as sample sizes increase.
5. Our approach uniquely models power generation and line flow constraints jointly as two-sided chance constraints. This comprehensive modelling ensures that all constraints are met with a predefined probability of compliance. Despite the influence of dataset size on computation time, our method includes strategic improvements that lessen this impact, thereby facilitating the efficient management of larger datasets without a corresponding increase in computational demand.

In the remainder of this paper. Section 3 describes the chance-constrained formulation of OPF. Section 4 presents the sample-based mixed integer programming reformulation and improvements. Section 5 illustrates the numerical results of our approach with benchmarks and another sample-based approach. Section 6 concludes this paper.

3 Chance-constrained OPF

3.1 Power system model formulation

With assumptions of neglecting thermal losses of power transmission, the same voltage magnitude and small voltage angle differences among buses, we consider DC linearization [26, 40, 48, 49] for the OPF problem in this paper. Let $\mathcal{B}, \mathcal{G}$ and $\mathcal{L}$ denote the set of buses, conventional generators and transmission branches of a system, respectively. Assume the total power mismatch between load and generation is Ω.

3.1.1 Power demand

The forecast of the load is used to estimate the uncertain power demand at each bus for OPF calculation, while inaccuracies exist. Therefore, the actual power demand on the ith bus $d_i(\omega)$ is modeled by its forecast load d_i with a fluctuation component ω_i as follows,

$$d_i(\omega) = d_i + \omega_i, \qquad \forall i \in \mathcal{B}, \tag{1}$$

where the sum of fluctuations on every bus is the total power mismatch of the system $\Omega = \sum_{i\in\mathcal{B}} \omega_i$. In addition, as power generation from renewable energies is often uncontrollable, we model it as a negative load in this paper. For the ith bus, the forecast generation is $-d_i$ and the forecast error is $-\omega_i$.

3.1.2 Power generation

Since the load model includes renewable power generation, we model only the generation from conventional power plants. For the ith bus, the actual power generation $g_i(\omega)$ is composed of a scheduled generation and the action of AGC as follows,

$$g_i(\omega) = g_i - \beta_i\Omega, \qquad \forall i \in \mathcal{G}, \tag{2}$$

where the scheduled generation g_i provides a referencing operating point, and we use an affine control policy $\beta_i\Omega$ to model the action of AGC system [40], such that the power mismatch can be compensated. Here, the participation factor β_i takes a value from 0 to 1, which represents the portion of energy that the ith generator would contribute to the total mismatch. A classic approach to determine the participation factor β_i is based on the proportion of its maximum generation capacity to the total. We optimise both the scheduled generation g_i and the participation factor β_i in our formulation.

3.1.3 Power flow

The power flow across transmission lines can be evaluated directly with the voltage angle difference and the line susceptance. To reduce the number of variables, we introduce a linear sensitivity, i.e., the power transmission distribution factor (PTDF) [50], to calculate the power flow. The solution obtained by the PTDF is equivalent to alternative approaches using voltage angles at every bus [35]. We denote this solution as Φ, which is an $|\mathcal{L}| \times |\mathcal{B}|$ matrix that correlates the injection of power with line flows. Thus, by denoting $ij \in \mathcal{L}$ as the line connecting buses i and j, the power flow at each branch can be written as follows,

$$f_{ij}(\omega) = \left[\Phi \cdot (g(\omega) - d(\omega))\right]_{ij}, \qquad \forall ij \in \mathcal{L}. \tag{3}$$

3.2 Uncertain variables

The uncertain variable ω_i represents the load and renewable generation forecast error, and $\Omega = \sum_{i\in\mathcal{B}} \omega_i$. A straightforward approach is to input scaled real-world data without any assumptions [10, 32]. With a large number of samples, this approach can provide the most realistic solution. However,

it is also possible that there is a limitation for sample size and that additional scenarios must be generated. The previous work [6, 31] suggested generating uncertain variables from an assumed multivariate normal distribution. In contrast, since the uncertain load and renewable generations are stochastic, an assumed distribution introduces additional uncertainties.

Another approach is to implement forecasting techniques for additional scenario generation. The main forecasting models include physical models that are built based on the actual environment and statistical models that forecast based on available past data. It is possible to build a physical model for a specified system, while with the increase of system size, there is an extremely large number of variables to be calibrated [51]. More importantly, as the model is build-to-spec, it is not able to implement any other cases. The purpose of this work is to develop a generic model that can be directly applied, and the use of statistical models is more practical. Since the OPF problems are solved in a short amount of time, it would be beneficial to consider a short-term wind power forecast technique, and Gaussian Process regression (GPR) is a viable approach [52].

GPR is mostly used to provide forecast information based on historical information. We adopt this method to generate additional scenarios for our case studies. Firstly, we take the scale real-world data and treat it as a random variable $\mathbf{x}$. Then, a Gaussian process (GP) is specified by its mean function and covariance function [53]. The mean function and covariance matrix of a real process $f(\mathbf{x})$ are defined as follows,

$$\begin{aligned} m(\mathbf{x}) &= \mathbb{E}\big[f(\mathbf{x})\big], \\ k\big(\mathbf{x}, \mathbf{x}'\big) &= \mathbb{E}\big[(f(\mathbf{x}) - m(\mathbf{x}))\big(f\big(\mathbf{x}'\big) - m\big(\mathbf{x}'\big)\big)\big]. \end{aligned} \tag{4}$$

For simplicity, we preprocess the data to set the mean function to zero. Let $K(X, X)$ denote a covariance matrix evaluated at all pairs of training instances and $[K(X,X)]_{ij} = k\big(x_i, x_j\big)$. $K\big(X, X_*\big)$ denotes a covariance matrix evaluated at all pairs of training and test instances. $K\big(X_*, X\big)$ and $K\big(X_*, X_*\big)$ are defined likewise. Then, the joint distribution of observed targets, say, the vector y, and the function values at the test locations, say, the vector f_*, is

$$\begin{bmatrix} \mathbf{y} \\ \mathbf{f}_* \end{bmatrix} \sim N\left(\mathbf{0}, \begin{bmatrix} \mathbf{K}(\mathbf{X}, \mathbf{X}) + \sigma_n^2 \mathbf{I} & \mathbf{K}\big(\mathbf{X}, \mathbf{X}_*\big) \\ \mathbf{K}\big(\mathbf{X}_*, \mathbf{X}\big) & \mathbf{k}\big(\mathbf{X}_*, \mathbf{X}_*\big) \end{bmatrix}\right), \tag{5}$$

where $\varepsilon \sim (0, \sigma_n^2)$ denotes independent, identically distributed noise to the observations, i.e., $y = f(x) + \varepsilon$. Then, the mean of the forecast value $\mathbf{f}_*$ is evaluated as follows,

$$\bar{\mathbf{f}}_* = \mathbf{K}\big(\mathbf{X}_*, \mathbf{X}\big)\big[\mathbf{K}(\mathbf{X}, \mathbf{X}) + \sigma_n^2 \mathbf{I}\big]^{-1} \mathbf{y}. \tag{6}$$

Last, the training process sets the GP parameters by maximizing the log marginal likelihood,

$$\begin{aligned} \log p(\mathbf{y}|\mathbf{X}) = &-\frac{1}{2}\mathbf{y}^T\big(\mathbf{K}(\mathbf{X}, \mathbf{X}) + \sigma_n^2 \mathbf{I}\big)^{-1}\mathbf{y} \\ &- \frac{1}{2}\log\left|\mathbf{K}(\mathbf{X}, \mathbf{X}) + \sigma_n^2 \mathbf{I}\right| - \frac{N}{2}\log 2\pi, \end{aligned} \tag{7}$$

where N is the number of training instances. The work in [53] shows that the marginal likelihood incorporates a trade-off between model fit and model complexity automatically.

3.3 Joint chance-constrained OPF

In a power system, the failure of the transmission line usually occurs gradually with the heating due to overloading. Hence, violations of line flow constraints may not be unacceptable for power providers. Moreover, these violations could be economically beneficial as long as they are controlled under a secure level; therefore, we consider them "soft constraints". Thus, we model them as CCs with a prescribed violation probability ϵ.

Our objective is to minimize the total operational cost $\text{Cost}(g_i, \beta_i, \Omega)$. Considering a generic linear cost function, the joint chance-constrained OPF is formulated as follows,

$$\min_{g_i, \beta_i} \quad \sum_{i \in \mathcal{G}} \text{Cost}(g_i, \beta_i, \Omega) \tag{8a}$$

$$\text{s.t.} \quad \sum_{i \in \mathcal{G}} g_i - \sum_{j \in \mathcal{B}} d_j = 0, \tag{8b}$$

$$\sum_{i \in \mathcal{G}} \beta_i = 1, \tag{8c}$$

$$0 \le \beta_i \le 1, \qquad \forall i \in \mathcal{G}, \tag{8d}$$

$$\mathbb{P}\left(\begin{matrix} f_{ij}^{\text{LB}} \le f_{ij}(\omega) \le f_{ij}^{\text{UB}}, & \forall ij \in \mathcal{L} \\ g_i^{\text{LB}} \le g_i(\omega) \le g_i^{\text{UB}}, & \forall i \in \mathcal{G} \end{matrix}\right) \ge 1 - \epsilon. \tag{8e}$$

Since the cost of generation varies for each generator, we optimise both the scheduled generation g_i and the participation factor β_i for each conventional generator. Unlike the CCs, the power balance is mandatory for the system, and therefore, we consider the associated constraints (8b) and (8c) as "hard constraints". As the participation factor compensates for the fluctuations, we ensure the balance of total power mismatch by (8c). Therefore, the constraint of power balance (8b) consists of the scheduled power only. Equation (8d) indicates that the participation factor takes a value between 0 and 1. Equation (8e) describes the joint CCs for both line flow and generation. Here, we denote by a^{LB} and a^{UB} the lower and upper bounds for a, respectively. The power flow among line ij and generation of the ith generator are constrained between their lower and upper bounds.

Constraints of line flow and generation are required to be satisfied jointly with an acceptance probability of $1-\epsilon$.

4 Mixed integer programming reformulation

The joint CCs (8e) usually cannot be evaluated directly. Since historical data for the power system are often available, we can estimate the empirical distribution of the probabilistic constraint (8e) via SAA. For simplicity, let $m = 2|\mathcal{G}| + 2|\mathcal{L}|$, we denote (8e) as follows,

$$\mathbb{P}\big(c_j(g_i, \beta_i, \omega) \le 0\big) \ge 1-\epsilon, \qquad \forall i \in \mathcal{B} \tag{9}$$

where for $j = 1, \ldots, m$, $c_j(g_i, \beta_i, \omega)$ takes one of the following forms,

$$\begin{aligned} &f_{ij}^{\mathrm{LB}} - f_{ij}(\omega) \le 0, \quad \forall ij \in \mathcal{L}, \\ &f_{ij}(\omega) - f_{ij}^{\mathrm{UB}} \le 0, \quad \forall ij \in \mathcal{L}, \\ &g_i^{\mathrm{LB}} - g_i(\omega) \le 0, \quad \forall i \in \mathcal{G}, \\ &g_i(\omega) - g_i^{\mathrm{UB}} \le 0, \quad \forall i \in \mathcal{G}. \end{aligned} \tag{10}$$

There are a total of m constraints that must be jointly satisfied with an acceptance probability $1-\epsilon$.

In Fig. 1, we present the block diagram of our approach, illustrating the sequence of steps taken to solve the modified IEEE test cases using our proposed model. The process begins with uncertainty modelling, where historical data is initially loaded to understand the variability and trends in power system operations. GPR is then applied to this historical data to model the uncertainty and generate additional scenarios for the system uncertain variables.

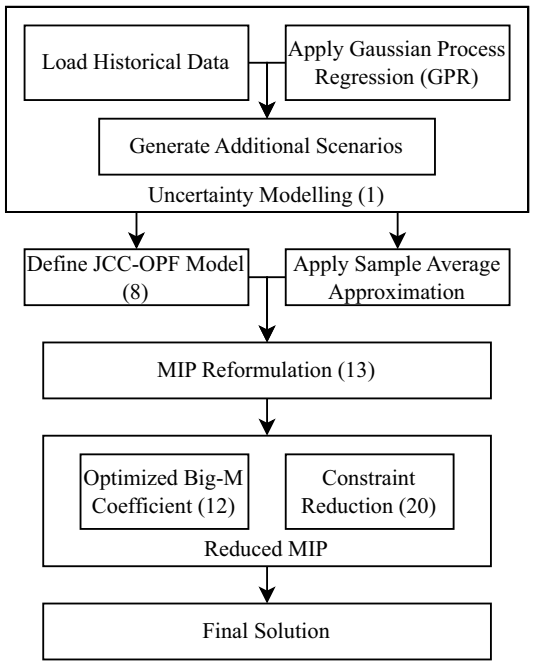

Fig. 1 Block diagram of the proposed methodology

Next, the JCC-OPF model is defined, incorporating the uncertain variables derived from the uncertainty modelling step. This model ensures that the system operates reliably under different scenarios. The SAA method is then applied to these scenarios, transforming the probabilistic constraints into deterministic ones and facilitating a more tractable problem formulation.

The deterministic MIP reformulation obtained from SAA can be solved using standard optimisation techniques. To enhance the efficiency of the MIP model, an optimised Big-M coefficient tightening technique is applied, improving computational performance and ensuring numerical stability. Additionally, a constraint reduction technique is implemented to improve the solution time by reducing the number of constraints, making the problem more computationally efficient without significantly sacrificing accuracy.

Finally, the reduced MIP model is solved using a branch-and-bound method, as implemented in the Gurobi solver. This step provides the final solution, optimising the power flow while considering the uncertainties and maintaining the prescribed power flow risk limits. This methodical flow ensures a robust and efficient approach to solving the OPF problem under uncertainty, providing a reliable and practical solution for real-world power systems. Additionally, a pseudo code for our problem-solving approach is provided in the Appendix to offer further clarity on the implementation details.

4.1 Sample average approximation

Without loss of generality, we take a generic example for illustration. The constraints $c_j(g_i, \beta_i, \omega) \le 0, j = 1, \ldots, m$ must be satisfied with an acceptance probability $1-\epsilon$. If the uncertain variable ω is available in a realization set $\{\omega^1, \ldots, \omega^N\}$, to satisfy the CC in the empirical distribution, at least $\lceil N(1-\epsilon)\rceil$ scenarios need to be satisfied, where $\lceil a \rceil$ is the smallest integer that is larger than or equal to a real number a. Therefore, by introducing a binary variable y^k and a sufficiently large positive number M_j^k that satisfies $c_j(g_i, \beta_i, \omega^k) \le M_j^k$ for each scenario k, we have,

$$c_j(g_i, \beta_i, \omega^k) \le y^k M_j^k, \quad \forall k = 1, \ldots, N, \tag{11a}$$

$$\sum_{k=1}^{N} y^k \le \lfloor N\epsilon \rfloor, \tag{11b}$$

$$y^k \in \{0, 1\}, \quad \forall k = 1, \ldots, N, \tag{11c}$$

where $\lfloor a \rfloor$ denotes the largest integer that is smaller than or equal to a real number a.

Equation (11a) represents the approximation of samples $k = 1, \ldots, N$. In the case of no constraint violation, $y^k = 0$ is allowed as $c_j(g_i, \beta_i, \omega^k) \leq 0$. In the case of $c_j(g_i, \beta_i, \omega^k) > 0$, we must set $y^k = 1$, such that $c_j(g_i, \beta_i, \omega^k) \leq M_j^k$, and (11a) is satisfied. The total number of constraint violations is limited by (11b). Hence, the prescribed violation probability ϵ can be maintained.

It is critical to choose the value of the big-M coefficient, such that the constraint does not cut-off the feasible region while maintaining a strong relaxation. For the kth scenario and the jth row, we determine the big-M coefficient with single scenario optimisation as follows,

$$\begin{aligned} M_j^k := \max_{g_i, \beta_i} \quad & c_j(g_i, \beta_i, \omega^k) \quad \forall i \in \mathcal{G}, \\ \text{s.t.} \quad & \text{Eqns. (8b)-(8d).} \end{aligned} \tag{12a}$$

Similarly, the original JCC-OPF can be approximated as follows,

$$\min_{g_i, \beta_i} \quad \sum_{i \in \mathcal{G}} \text{Cost}(g_i, \beta_i, \Omega) \tag{13a}$$

$$\text{s.t.} \quad g_i^{\text{LB}} - g_i(\omega^k) \leq y^k M_j^k, \quad \forall i \in \mathcal{G}; k = 1, \ldots, N, \tag{13b}$$

$$g_i(\omega^k) - g_i^{\text{UB}} \leq y^k M_j^k, \quad \forall i \in \mathcal{G}; k = 1, \ldots, N, \tag{13c}$$

$$f_{ij}^{\text{LB}} - f_{ij}(\omega^k) \leq y^k M_j^k, \quad \forall ij \in \mathcal{L}; k = 1, \ldots, N, \tag{13d}$$

$$f_{ij}(\omega^k) - f_{ij}^{\text{UB}} \leq y^k M_j^k, \quad \forall ij \in \mathcal{L}; k = 1, \ldots, N, \tag{13e}$$

$$\sum_{k=1}^{N} y^k \leq N\epsilon, \tag{13f}$$

$$y^k \in \{0, 1\}, \quad \forall k = 1, \ldots, N, \tag{13g}$$

Eqns. (8b)-(8d).

The JCC is approximated with $Nm + 1$ linear constraints with an introduction of N binary variables. This reformulated OPF model (13) can be efficiently solved using off-the-shelf solvers, such as Gurobi [54].

In the implementation of the SAA method within our study, we draw upon the theoretical framework detailed by [47], particularly as detailed in Section 2.2 of [47]. This section offers an in-depth theoretical analysis of the SAA method, with a focus on the probabilistic estimation of feasible regions. It highlights how the sample approximation feasible region can reliably approximate the true feasible region, which is vital for ensuring that solutions derived from the SAA method are applicable to real-world constraints. Essentially, an MIP problem is NP-hard. Furthermore, the detailed computational cost analysis of the SAA method for different complexities can be referred to Section 3.6 of [55] and Section 5 of [56]. These findings have directly influenced our approach to implementing the SAA method to address the complexities of power system operations, ensuring our solutions are both accurate and feasible.

Moreover, the thorough numerical experiments in [47] demonstrated the practical viability of SAA in handling large sample sizes and the corresponding computational considerations. Their findings, particularly on the computational effort required for large sample sizes (e.g., $N = 10,000$), guide our methodological choices, balancing computational intensity with solution quality.

Our research takes these theoretical and empirical insights and applies them to novel challenges in power systems. We tailor the SAA approach to address specific power system optimisation problems, ensuring that our methodology is not only theoretically robust but also practically relevant. Our novel contributions lie in extending and refining these foundational principles to cater to the unique demands of power systems optimization, thus bridging the gap between theoretical rigour and real-world applicability.

This section, therefore, not only reiterates the theoretical basis of our approach, drawing from the seminal work of [47], but also outlines our advancements beyond this groundwork. It underscores our commitment to leveraging established methodologies while pushing the boundaries of innovation in power system optimisation.

4.2 Model improvement

The SAA method provides an approach to approximate the CCs by the utilisation of past scenario data. Although the reformulated MIP can be solved with off-the-shelf solvers, it is essentially an NP-hard problem [56]. With the increasing number of scenarios, the number of binary variables and constraints increases accordingly. Therefore, this may lead to a significant increase in the computation time. To ease such an effect, we improve a constraint strengthening strategy that was first proposed in [57].

4.2.1 Power generation constraints

We use the lower bound power generation constraint as an example. First, we put the terms that vary by scenario at the right-hand side (rhs) by rearranging the constraint as follows,

$$g_i^{LB} - g_i \le M_j^k y^k - \beta_i \Omega^k. \tag{14}$$

Note that the value of the decision variable β_i does not change with respect to the scenario number k, i.e., the rhs depends only on the value of the uncertain variable Ω^k. For the values of $\Omega^k, k = 1, \dots, N$, we obtain a permutation σ by sorting them in a nonascending order,

$$\Omega^{\sigma_1} \ge \Omega^{\sigma_2} \ge \cdots \ge \Omega^{\sigma_N}. \tag{15}$$

In addition, the cardinality constraint (11b) implies that there is at most $\lfloor N\epsilon \rfloor$ scenarios of constraint violation. Let

$$p = 1 + \lfloor N\epsilon \rfloor. \tag{16}$$

For case $k \le p$, there exists at least one scenario of $y^k = 0$. Moreover, as the uncertain term Ω^k has been rearranged in nonascending order, if binary variable $y^k = 0$ appears for $k \le p$, the remaining constraints $g_i^{LB} - g_i \le M_j^k y^k - \beta_i \Omega^k$ with $k > p$ are redundant. For every power generation CC in the joint CCs, the number of constraints can be reduced from N to p. We denote $\mathcal{P}^{gl}$ as the set of the first p elements of the permutation for the power generation lower bound constraints, respectively, i.e., $\mathcal{P}^{gl} = \{\sigma_1, \sigma_2, \dots, \sigma_p\}$, $\mathcal{P}^{gu}$ in a similar way.

In practice, we know that the higher the load is, the higher the power generation per plant is. Note that the uncertain term Ω is the total power mismatch, representing the difference between the actual load and the forecast. For the lower bound constraint, as the scenarios with higher values of Ω result in a higher value of power generation, they are less likely to lead to constraint violation. Hence, for the lower bound power generation constraints, the solutions of decision variables are more sensitive to a lower value of Ω.

4.2.2 Power flow constraints

The reduction technique cannot be directly implemented to the power flow constraints. However, based on a similar idea, we can obtain a relaxation of the original MIP by removing a large number of constraints. We take the lower bound flow constraint as an example. Similarly, the rearranged flow constraint is written as follows,

$$f_{ij}^{LB} - \phi_{(ij,\cdot)} g \le M_j^k y^k - \phi_{(ij,\cdot)} \boldsymbol{\beta} \Omega^k - \phi_{(ij,\cdot)} d(\omega)^k, \tag{17}$$

where $\phi_{(ij,\cdot)}$ denotes the ijth row of the PTDF matrix.

In this case, the terms $-\phi_{(ij,\cdot)}\boldsymbol{\beta}\Omega^k$ and $-\phi_{(ij,\cdot)}d(\omega)^k$ on the rhs change by the scenario number k, where $\phi_{(ij,\cdot)}\boldsymbol{\beta}\Omega^k$ represents the change of power flow on the ijth line with regards to the action of AGC, and where $\phi_{(ij,\cdot)}d(\omega)^k$ represents the change of power flow on the ijth line with regards to the load. Unlike the previous case, $\phi_{(ij,\cdot)}\boldsymbol{\beta}\Omega^k$ involves a decision variable $\boldsymbol{\beta}$ and its value may vary when $\boldsymbol{\beta}$ varies. Moreover, the summation of $\phi_{(ij,\cdot)}\boldsymbol{\beta}\Omega^k$ and $\phi_{(ij,\cdot)}d(\omega)^k$ may have different orders with each of $\phi_{(ij,\cdot)}\boldsymbol{\beta}\Omega^k$ and $\phi_{(ij,\cdot)}d(\omega)^k$. It is more likely that the indices associated with larger scenarios of $\phi_{(ij,\cdot)}\boldsymbol{\beta}\Omega^k$ and $\phi_{(ij,\cdot)}d(\omega)^k$ with respect to k will yield the larger $\phi_{(ij,\cdot)}\boldsymbol{\beta}\Omega^k + \phi_{(ij,\cdot)}d(\omega)^k$. Our relaxation in this section is motivated by this idea.

We sort Ω^k and $\phi_{(ij,\cdot)}d(\omega)^k$ as follows,

$$\Omega^{\sigma_1} \ge \Omega^{\sigma_2} \ge \cdots \ge \Omega^{\sigma_N}, \tag{18}$$

$$\phi_{(ij,\cdot)}d(\omega)^{\delta_1} \ge \phi_{(ij,\cdot)}d(\omega)^{\delta_2} \ge \cdots \ge \phi_{(ij,\cdot)}d(\omega)^{\delta_N}. \tag{19}$$

Since the term $-\phi_{(ij,\cdot)}\boldsymbol{\beta}\Omega^k$ is associated with decision variable $\boldsymbol{\beta}$, depending on the value of $\boldsymbol{\beta}$, it is possible that the coefficient $\phi_{(ij,\cdot)}\boldsymbol{\beta}$ of uncertain variable Ω^k is negative. Therefore, both the αp largest and the αp smallest Ω^k from (18) can be candidates for the largest αp scenarios of $\phi_{(ij,\cdot)}\boldsymbol{\beta}\Omega^k$, and we denote α as a relaxation factor for p to represent the scenarios that we consider.

Moreover, note that the permutations σ_i and δ_i may not be the same. For the term $-\phi_{(ij,\cdot)}d(\omega)^k$, scenarios from the first αp elements of the permutation $\{\delta_1, \delta_2, \dots, \delta_N\}$ must be considered. In the meantime, as the two uncertain terms are added together, we expand our feasible region by doubling the considered scenarios, i.e., set $\alpha = 2$. Hence, we denote by $\mathcal{P}^{\Omega}$ the index set containing the first and last $2p$ elements of the permutation (18), i.e., $\mathcal{P}^{\Omega} = \{\sigma_1, \sigma_2, \dots, \sigma_{2p}, \sigma_{N-2p+1}, \sigma_{N-2p+2}, \dots, \sigma_N\}$, and denote by $\mathcal{P}_{ij}^{fl}$ the index sets of first $2p$ elements of the permutation for the lower bound of $\phi_{(ij,\cdot)}d(\omega)^k$, i.e., $\mathcal{P}_{ij}^{fl} = \{\delta_1, \delta_2, \dots, \delta_{2p}\}$, and by $\mathcal{P}_{ij}^{fu}$ the upper bound of $\phi_{(ij,\cdot)}d(\omega)^k$ in a similar way. For the lower bound constraint, we consider the scenarios $k \in \mathcal{P}^{\Omega} \cup \mathcal{P}_{ij}^{fl}$. Since both the signs of the term $-\phi_{(ij,\cdot)}\boldsymbol{\beta}\Omega^k$ are considered, for the upper bound constraint, we consider the scenarios $k \in \mathcal{P}^{\Omega} \cup \mathcal{P}_{ij}^{fu}$. The number of every power flow constraint can be reduced from N to $6p$. The price is that we relax the feasible region in (13d) and (13e).

In summary, we propose a relaxation of (13) that reduces the number of every power generation CC to p and the number of power flows CC to $6p$,

$$\min_{g_i, \beta_i} \quad \sum_{i \in \mathcal{G}} \text{Cost}(g_i, \beta_i, \Omega) \tag{20a}$$

$$\text{s.t.} \quad g_i^{\text{LB}} - g_i(\omega^k) \le y^k M_j^k, \quad \forall i \in \mathcal{G}; k \in \mathcal{P}^{gl}, \tag{20b}$$

$$g_i(\omega^k) - g_i^{\text{UB}} \le y^k M_j^k, \quad \forall i \in \mathcal{G}; k \in \mathcal{P}^{gu}, \tag{20c}$$

$$f_{ij}^{\text{LB}} - f_{ij}(\omega^k) \le y^k M_j^k, \quad \forall ij \in \mathcal{L}; k \in \mathcal{P}^{\Omega} \cup \mathcal{P}_{ij}^{fl}, \tag{20d}$$

$$f_{ij}(\omega^k) - f_{ij}^{\mathrm{UB}} \le y^k M_j^k, \quad \forall ij \in \mathcal{L}; k \in \mathcal{P}^{\Omega} \cup \mathcal{P}_{ij}^{fu}, \tag{20e}$$

Eqns. (18b)-(18d), and (13f)-(13g).

Since the violation probability ϵ is often small, p and $6p$ are small when compared to N. That is, our relaxation can remove many constraints. Our simulation results in Sect. 5.1 indicate that the relaxation is quite tight compared to that of the original MIP (13).

4.3 Model comparison

Our model leverages historical scenario data to manage uncertainty, similar to the scenario approach (SA) [58] and robust constraints (RC) approach [59]. Like our approach, SA utilises past data but pairs it with a robust optimisation technique. The difference is that the robust optimisation (RO) technique does not allow for constraint violation, and that the solution is robust to all the scenarios it has considered. As a result, SA with traditional RO is more computationally efficient, while the obtained solution may be overly conservative.

The work [28] modelled the uncertain renewable generation and load reserve to formulate a multi-period CC OPF. The authors adopted a probabilistically RO technique to ensure a priori probability guarantee with a large number of samples considered [28]. Similarly, we determine a certain number of scenarios as N^{SA}. All of the N^{SA} past scenarios must be satisfied. The following equation is adopted to obtain N^{SA},

$$N^{\mathrm{SA}} \ge \frac{2}{\alpha}\left(\ln\left(\frac{1}{\epsilon}\right) + n\right), \tag{21}$$

where α is chosen as 1×10^{-4}, ϵ is the risk level as defined in (8e), and n is the number of decision variables. Our approach optimizes the scheduled generation and participation factor, which is twice of the number of generators.

The RC approach, on the other hand, approximates CCs with robust constraints that form a robust optimisation problem, constructed from historical data. This reformulation replaces probabilistic constraints with a worst-case scenario framework,

$$\begin{aligned} f_{ij}^{\mathrm{LB}} &\le \min_{\omega \in \mathcal{U}} f_{ij}(\omega), \quad \max_{\omega \in \mathcal{U}} f_{ij}(\omega) \le f_{ij}^{\mathrm{UB}}, \quad \forall ij \in \mathcal{L}, \\ g_i^{\mathrm{LB}} &\le \min_{\omega \in \mathcal{U}} g_i(\omega), \quad \max_{\omega \in \mathcal{U}} g_i(\omega) \le g_i^{\mathrm{UB}}, \quad \forall i \in \mathcal{G}, \end{aligned} \tag{22}$$

where $\mathcal{U}$ represents the uncertainty set derived from historical data.

To further substantiate the robustness and effectiveness of the proposed model, we extend our comparison to include a more advanced framework, the DR CC-OPF, as detailed in [60]. This model distinguishes itself by leveraging the DRO methodology for the reformulation of CCs. Unlike traditional RO, DRO does not presume full knowledge of the underlying probability distributions. Instead, it operates under the assumption that the true distribution of historical data is unknown, yet it falls within a predefined ambiguity set of distributions. For our comparison, we adopt the boxed-based ambiguity set approach, as outlined by [60], utilising uncertain historical data to define the set. We formulate the corresponding joint chance constraint as follows,

$$\inf_{\mathbb{P} \in \mathcal{P}} \mathbb{P}\begin{pmatrix} f_{ij}^{\mathrm{LB}} \le f_{ij}(\omega) \le f_{ij}^{\mathrm{UB}}, & \forall ij \in \mathcal{L} \\ g_i^{\mathrm{LB}} \le g_i(\omega) \le g_i^{\mathrm{UB}}, & \forall i \in \mathcal{G} \end{pmatrix} \ge 1 - \epsilon, \tag{23}$$

where $\mathcal{P}$ represents the ambiguity set that we are considering.

This comparison is crucial for demonstrating the efficacy and efficiency of our model, particularly its ability to manage uncertainties with potentially less conservative and better objective values. By comparing these models, we aim to illustrate the practical benefits of our approach to power system management under uncertainty, emphasising its superiority in balancing solution quality with computational resources.

5 Case studies

Numerical experiments are performed for the proposed model. Since the standard IEEE test cases assume infinite line flow limits, in our case study, we use the modified "IEEE 14-", "57-", and "118-bus" systems from the | pglib-opfl package [61]. In such a way, prescribed line flow limits are associated.

We use the off-the-shelf solver Gurobi to solve our MIP reformulation. Branch-and-bound method is used for the solving process of our reformulation [54]. The computation time is referred to as the time taken for the solver to obtain a feasible solution with an objective value associated with an MIP gap of less than 0.01%, which is the difference between the lower and upper bounds of the objective.

A demonstration of model improvement is presented via the comparison of computation time. To assess the performance and robustness of the proposed model, ten replications with different numbers of uncertain scenarios for all three systems are conducted. Last, a comparison with deterministic [62], SA, RC, and DRO models [58] is performed.

5.1 Model improvement

The improvement of model solvability is mainly illustrated by the computation time for solving the MIP to a certain tolerance. Since the 118-bus system is the most complex case that we consider, it will require the most time to solve,

and we choose it to demonstrate the effectiveness of our model improvement strategy. We generate ten uncertainty sets for different numbers of scenario sets. Three models with fixed big-M coefficients, predetermined big-M coefficients, and reduced CCs are run with the generated uncertainty sets. To ensure the accuracy of the aforementioned models, the objective values and decision variables are cross-checked.

5.1.1 Choice of big-M

The introduction of the big-M coefficient in our formulation relaxes our model to allow constraint violation of the JCC. We use (12) to determine an appropriate value that is not too large to form a weak relaxation but not too tight to cut-off any feasible region.

Figure 2 illustrates the improvement of computation time when the big-M coefficients are tightened. Overall, out of ten sets of uncertainties, the mean computation time required to solve the model is reduced.

5.1.2 Constraint reduction

Figure 3 illustrates the reduction of computation time after applying the constraint reduction techniques. This is reasonable as there are fewer constraints to be considered. Additionally, as the boxplot reveals the dispersion of the model run time, most of the computation time was reduced in a tight range. Moreover, since the MIP problem is NP-hard, the computation time is more significant with the increase in considered scenarios, while the effect of time reduction is more pronounced.

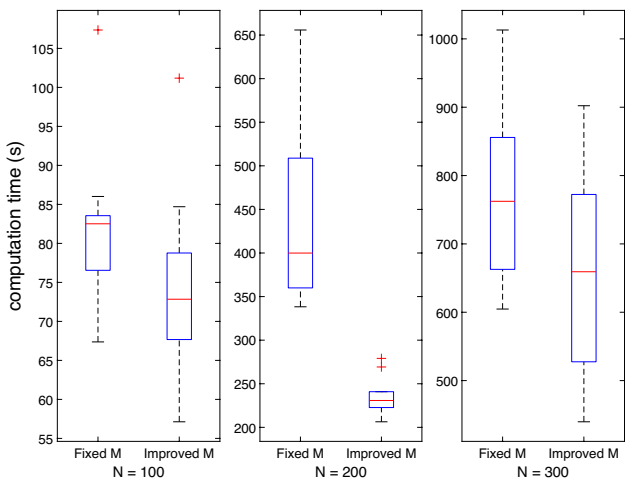

Fig. 2 Comparison of 118-bus system CC-OPF with different big-M coefficients. *N*: number of considered scenarios

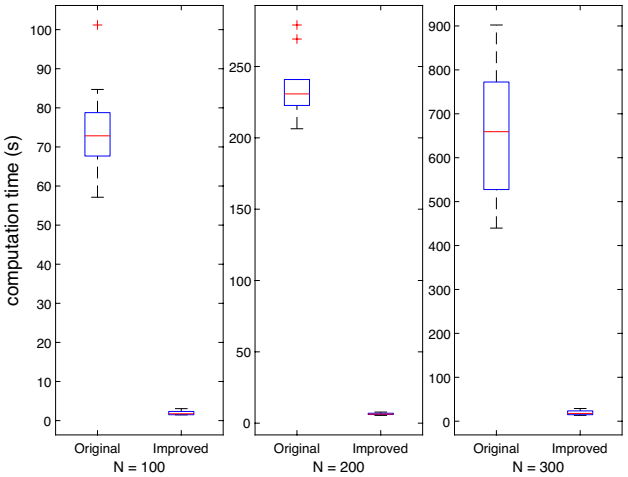

Fig. 3 Comparison of 118-bus system CC-OPF before and after constraint reduction. *N*: number of considered scenarios

5.2 Performance with different scenario numbers

Since our approach uses realistic scenario data directly, it is important to assess the performance of the proposed model with different numbers of scenarios. Out of ten replications, Table 2 records the minimum, average, and maximum values for the objective value, in-sample feasibility and computation time for 100, 200, 300, and 500 scenarios.

From Table 2, it can be seen that, as the number of considered scenarios increases, the range of objective values converges, i.e., out of ten replications, the objective values are less dispersed, the obtained solution would be more robust. The in-sample feasibility is referred to *prob* in Table 2, where the actual constraint violation probability ϵ_{actual} can be calculated by $1 - prob$. For small systems with 14 or 57 buses, some of the in-sample feasibility are 1. This indicates that there is no constraint violation for the associated uncertainty dataset, and the solution is robust to all the considered scenarios. With an increase in the bus number, the dimension of the decision variables and CCs increases, the system becomes more complex, and the feasibility decreases. Nevertheless, as the CCs are constrained with a prescribed violation probability ϵ as (8e), the in-sample feasibility is always maintained beyond the prescribed acceptance level of 95%. Finally, the computation time required to solve the OPF increases when the bus number and scenarios increase. The implementation of model improvement strategies reduces computation time significantly. For the 14- and 57-bus systems, it took less than one second to solve, while when the system is relatively large e.g., 118-bus system, the maximum computation time is 342 s. As such, in practice, since the OPF performs every 5–30 min for the power system, the consideration of 300–500 scenarios would be sufficient to provide acceptable results in a timely manner.

Table 2 Results of proposed model with feasibility and computation time

	N = 100	N = 200	N = 300	N = 500
14-bus				
Min. obj ($)	2040.8	2046.8	2047.8	2050.1
Avg. obj ($)	2050.9	2051.2	2052.1	2052.3
Max. obj ($)	2060.7	2055.2	2055.8	2054.2
Min. prob	1.000	1.000	1.000	1.000
Avg. prob	1.000	1.000	1.000	1.000
Max. prob	1.000	1.000	1.000	1.000
Min. time (s)	0.0390	0.0432	0.0563	0.0407
Avg. time (s)	0.0487	0.0616	0.0677	0.0494
Max. time (s)	0.0828	0.0760	0.0868	0.0705
57-bus				
Min. obj ($)	34,759	34,727	34,749	34,741
Avg. obj ($)	34,800	34,768	34,784	34,768
Max. obj ($)	34,858	34,794	34,814	34,799
Min. prob	0.950	0.970	0.977	0.982
Avg. prob	0.985	0.984	0.993	0.995
Max. prob	1.000	1.000	1.000	1.000
Min. time (s)	0.121	0.172	0.324	0.319
Avg. time (s)	0.134	0.193	0.438	0.531
Max. time (s)	0.156	0.228	0.579	0.733
118-bus				
Min. obj ($)	93,106	93,143	93,169	93,159
Avg. obj ($)	93,194	93,188	93,201	93,205
Max. obj ($)	93,254	93,247	93,235	93,229
Min. prob	0.950	0.950	0.950	0.950
Avg. prob	0.950	0.950	0.950	0.950
Max. prob	0.950	0.950	0.950	0.950
Min. time (s)	1.475	5.454	13.264	33.398
Avg. time(s)	1.929	6.498	18.870	93.140
Max. time (s)	3.063	7.782	28.958	341.985

5.3 Model comparison

Tables 3 and 4 illustrate the results similarly as in Table 2. However, we define out-of-sample feasibility as *prob* in them. This metric is determined by testing the feasibility of 10^6 additional uncertain scenarios against the obtained solutions. We use this metric to demonstrate the robustness of our proposed approach with some state-of-the-art models. For a comprehensive analysis, we choose our MIP approach with considerations of 300 and 500 scenarios for this comparison study. Specifically, we decide to perform the comparison studies for 14- and 57-bus systems with the deterministic OPF, SA and the RC model against our proposed model, as detailed in Table 3. To further demonstrate the effectiveness of our approach, we extend the comparison to include the DR approach for the 118-bus system, as depicted in Table 4. This structured comparison aims to showcase the

Table 3 Model comparison against the nominal and scenario approach

	Nominal	SA	RC	MIP (300)	MIP (500)
14-bus					
Min. obj ($)	–	2,461.5	2,051.6	2,047.8	2,050.1
Avg. obj ($)	2,051.5	2,489.0	2,062.5	2,052.1	2,052.3
Max. obj ($)	–	Inf	2,081.5	2,055.8	2,054.2
Min. prob	0.499	0	0.996	0.999	0.999
Avg. prob	0.500	0.993	0.999	0.999	0.999
Max. prob	0.501	0.994	0.999	0.999	0.999
Min. time (s)	–	0.0325	0.040	0.0563	0.0407
Avg. time (s)	0.175	0.0425	0.042	0.0677	0.0494
Max. time (s)	–	0.0492	0.049	0.0868	0.0705
57-bus					
Min. obj ($)	–	35,493	35,210	34,749	34,741
Avg. obj ($)	34,773	35,625	35,273	34,784	34,768
Max. obj ($)	–	Inf	35,327	34,814	34,799
Min. prob	0.000	0	0.994	0.978	0.982
Avg. prob	0.000	0.995	0.998	0.983	0.987
Max. prob	0.000	0.999	0.999	0.988	0.991
Min. time (s)	–	0.2228	0.409	0.324	0.319
Avg. time (s)	0.173	0.2776	0.414	0.438	0.531
Max. time (s)	–	0.3761	0.422	0.579	0.733

effectiveness and robustness of our proposed model across different system scales and against both conventional and advance optimisation methods.

5.3.1 IEEE 14-, 57-bus systems

The 'nominal' values, derived using the MATPOWER package [62], serve as a foundational benchmark, representing solutions to the deterministic OPF problem where uncertainty is considered null $\omega = 0$. It is also an approach that is widely used by utility companies.

From the objective value perspective, the nominal approach often yields the lowest mean cost under the assumption of no uncertainty. Our MIP approach, designed to accommodate certain degrees of constraint violations, tends to produce results with mean objectives that closely approximate the nominal, thereby highlighting its efficiency in handling uncertainties with minimal cost deviations. This adaptability contrasts with the SA and RC, which requires constraint satisfaction across all considered scenarios and often incurs higher total operational costs. Furthermore, our analysis reveals instances within ten replications where the SA method fails to provide a feasible solution, due to the impracticality of satisfying all scenarios, thus leading to 'inf' objective value and 0 feasibility. For clarity, these infeasible instances are excluded from our mean value calculations. Overall, the results of objective values underscore our

Table 4 Model comparison against the nominal and scenario approach 118-bus system

118-bus	Nominal	SA	RC	DRO	MIP (300)	MIP (500)
Min. obj ($)	–	118,304	95,123	101,153	93,169	93,159
Avg. obj ($)	93,133	122,553	95,290	104,887	93,201	93,205
Max. obj ($)	–	Inf	95,613	105,431	93,235	93,229
Min. prob	0.000	0	0.998	0.992	0.888	0.931
Avg. prob	0.000	0.996	0.998	0.995	0.916	0.949
Max. prob	0.000	0.997	1	0.998	0.934	0.975
Min. time (s)	–	21.222	374.029	14.688	13.264	33.398
Avg. time (s)	0.179	77.609	394.643	21.613	18.870	93.140
Max. time (s)	–	94.166	426.589	36.578	28.958	341.985

MIP approach's effectiveness, and demonstrate its capability to balance economic efficiency with operational robustness.

In conducting out-of-sample tests for our comparison studies, it is observed that not all solutions consistently meet the prescribed feasibility threshold of 0.95. Specifically, the nominal approach demonstrates limited feasibility for the simpler 14-bus system structure and is entirely infeasible for more complex systems. The limited feasibility for the 14-bus systems is due to the simplicity of the system configuration, where there are two active power generators and the balance between the total load of 259 MW and a generation capacity of 399 MW. In contrast, the SA and RC models leverage the RO techniques which encompass a broader spectrum of scenarios, generally exhibiting higher feasibility across all tested cases. Despite this, our MIP approach stands out, not only achieving out-of-sample feasibility rates exceeding 98% for both the 14- and 57-bus systems, but also presenting improved objective values when compared to the robust methods, illustrating its effectiveness in navigating uncertainty while optimising operational costs.

The analysis of computational efficiency reveals that the deterministic approach, with no consideration of uncertainty, stands out for its speed. In the context of the 14-bus system, the computation time difference between the state-of-the-art approaches and our MIP is minimal, reflecting efficiency in less complex scenarios. However, as the complexity of the system structure increases, we observe a gradual escalation in computation time. Specifically, our MIP approach exhibits a correlative increase in computation time as the complexity of the system and the number of scenarios considered rise.

5.3.2 IEEE 118-bus system

Table 4 presents the comparison results for the 118-bus system, extending our analysis beyond the scopes of the 14- and 57-bus systems. For this more complex system, we include the more advanced DR approach, which employs DRO techniques to reformulate chance constraints. The DRO models are solved using the Mosek optimiser and the associated actual computation time is reported [63].

In the analysis of the 118-bus system, the observed trends align with those identified in smaller systems. Our MIP approach is confirmed as the most cost-efficient method, achieving a notable cost advantage. Specifically, the MIP approach, with consideration of 300 scenarios, yields an average objective value of 93,201. In comparison, the DRO approach incurs a 12.5% higher cost, resulting in an average of 104,887, the RC approach incurs a cost similar to MIP, yet slightly higher. This difference underscores our MIP approach's cost benefits. The SA incurs the highest average operational cost at 122,553, underscoring its economic drawbacks compared to both MIP, RC, and DRO approaches.

The MIP approach not only excels in cost efficiency but also in computational performance. For the model considering 300 scenarios, it records an average computation time of 18.870 seconds, setting a benchmark for efficiency. In contrast, while SA and DRO achieve commendable computation time, they do not match the efficiency of MIP. The RC requires the most computational resources, primarily due to the increased size of the uncertainty set considered.

In conclusion, our comparison studies endorse the MIP approach as the superior methodology, providing an optimal balance between cost efficiency, operational robustness, and computational speed. The DRO approach emerges as a formidable alternative, offering a more cost-effective solution over SA while maintaining comparable robustness. However, when considering all factors, including cost, computation time, and out-of-sample feasibility, the MIP approach holds the best overall value under uncertainties.

5.3.3 Statistical analysis of model performance

To quantitatively assess the performance of our proposed MIP approach against the SA, RC, and DRO methods, we conduct a statistical analysis. This includes both a visual comparison using boxplots and a set of statistical tests.

Boxplots are generated to compare the objective values and computation time of the SA, RC, DRO and our MIP approach. Figure 4 presents these comparisons.

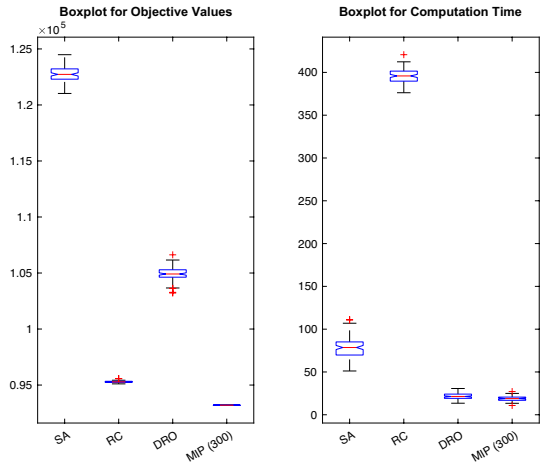

Fig. 4 Comparison of 118-bus system CC-OPF with different approaches

The boxplot of objective values clearly illustrates that our MIP approach consistently achieves better (lower) objective values compared to all the other methods. This visual representation underscores the economic efficiency of our approach.

Similarly, the boxplot for computation time demonstrates the computational efficiency of our method. Despite the complexity of the MIP approach, it exhibits competitive, if not faster, computation time compared to all the other methods.

Further, a *t*-test is performed to statistically compare the performance of the SA, RC, and DRO to the proposed MIP approach. The results of the *t*-tests for both objective values and computation time are significant (close to 0), confirming that the differences observed in the boxplot analysis are not due to random variation.

Overall, these statistical analyses provide strong evidence that our proposed MIP approach is not only more economically efficient but also computationally efficient compared to the SA, RC, and DRO methods. This underscores the viability of our approach to practical implementation in power system operations, balancing cost-effectiveness with computational feasibility.

6 Conclusion

This paper presented an MIP reformulation for the CC-OPF problem under uncertain load and renewable energy generation. The proposed methodology was tested on modified IEEE 14-, 57- and 118-bus systems, demonstrating its effectiveness in providing a lower-cost solution while maintaining system requirements with an acceptable probability.

Summary of contributions We introduced a novel SAA method to the JCC-OPF model, enhancing the traceability of the problem without compromising solution quality. Our method leverages historical data to formulate an MIP problem that can be solved by off-the-shelf solvers, mitigating the risks associated with distributional assumptions. We addressed the joint CCs in their entirety, avoiding overly conservative solutions by considering all constraints jointly. To tackle the challenge of increasing complexity, we implemented a model improvement strategy that significantly reduces the number of binary variables required, lowering the computational burden. Furthermore, our approach uniquely models power generation and line flow constraints jointly as two-sided CCs, ensuring compliance with a predefined probability.

Limitations Our approach relies on historical data to generate scenarios using GPR, which assumes the availability and quality of historical data. Sparse or poor-quality data can impact the accuracy of scenario generation. Additionally, the MIP reformulation, despite the constraint reduction technique, remains computationally intensive, particularly for large-scale power systems with many scenarios. This can limit real-time applicability. The use of DC linearisation simplifies the AC power flow equations but may not capture all the nuances of real power system behaviour, especially in systems with significant reactive power flow and voltage variations.

Future works It is necessary to explore more advanced scenario generation techniques, such as non-parametric methods or machine learning approaches, and collect more real-world data to improve the accuracy and reliability of generated scenarios. Extending our approach to AC-OPF models would provide a more accurate representation of power system behaviour, involving the development of efficient solution techniques for the nonlinear and nonconvex nature of AC power flow equations under uncertainty. Further reducing the computational burden could make our method more suitable for real-time applications, potentially involving more efficient algorithms, parallel processing techniques, or approximation methods. Future studies could also model and manage extreme events, such as natural disasters, which could significantly impact power system operations.

By addressing these limitations and pursuing these future research directions, we aim to further enhance the robustness, efficiency, and practicality of JCC-OPF solutions under uncertainty, contributing to the robust and cost-effective operation of power systems.

Appendix: Pseudo code

Algorithm 1 Algorithm implementation: Detailed pseudo code

Input: Forecasted load d_i, forecast error ω_i, power flow matrix Φ, generation limits g_i^{LB}, g_i^{UB}, line flow limits f_{ij}^{LB}, f_{ij}^{UB}, violation probability ϵ
Output: Optimised generation g_i and participation factor β_i
Initialise parameters and variables
Set the number of scenarios N
Generate scenarios ω^k for $k = 1, 2, \ldots, N$
for each scenario $k = 1, 2, \ldots, N$ **do**
    Generate scenario ω^k based on historical data
end for
for each scenario $k = 1, 2, \ldots, N$ **do**
    for each generator $i \in \mathcal{G}$ **do**
        Add constraint: $g_i^{LB} \leq g_i - \beta_i \Omega^k \leq g_i^{UB}$
    end for
    for each line $ij \in \mathcal{L}$ **do**
        Add constraint: $f_{ij}^{LB} \leq \Phi_{ij} \cdot (g(\omega^k) - d(\omega^k)) \leq f_{ij}^{UB}$
    end for
end for
for each constraint $j = 1, \ldots, m$ **do**
    Introduce binary variable y^k
    Add constraint: $c_j(g_i, \beta_i, \omega^k) \leq y^k M_j^k$
    Add cardinality constraint: $\sum_{k=1}^{N} y^k \leq \lfloor N\epsilon \rfloor$
end for
for each generator $i \in \mathcal{G}$ **do**
    Identify the most binding constraints P_{gl} and P_{gu}
    Add reduced constraints: $g_i^{LB} \leq g_i(\omega^k) \leq g_i^{UB}, \forall k \in P_{gl} \cup P_{gu}$
end for
for each line $ij \in \mathcal{L}$ **do**
    Identify the most binding constraints P_{fl} and P_{fu}
    Add reduced constraints: $f_{ij}^{LB} \leq f_{ij}(\omega^k) \leq f_{ij}^{UB}, \forall k \in P_{fl} \cup P_{fu}$
end for
Optimisation:
Solve the MIP problem (20) using off-the-shelf solver (i.e., Gurobi)
Obtain optimised values g_i and β_i
Return optimised generation g_i and participation factor β_i

Authors' contributions All authors contributed to the study conception and design. Material preparation, data collection, modeling and analysis were performed by JQ, RJ, HM, and DD. The manuscript was mainly written by JQ and all authors commented on the manuscript. All authors read and approved the manuscript.

Funding Open Access funding enabled and organized by CAUL and its Member Institutions. This work is partly supported by the UNSW Global Research and Innovation Partnerships Grant and the ARC Research Hub for Integrated Energy Storage Solutions (RG173052).

Data availability The datasets generated during and/or analysed during the current study are available on requested.

Declarations

Conflict of interests The authors have no relevant financial or non-financial interests to disclose.

References

1. Xu J, Liu B, Mo H, Dong D (2021) Bayesian adversarial multi-node bandit for optimal smart grid protection against cyber attacks. Automatica 128:109551
2. Chen X, Lin J, Liu F, Song Y (2019) Optimal control of AGC systems considering non-Gaussian wind power uncertainty. IEEE Trans Power Syst 34(4):2730–2743
3. Xu Y, Mili L, Sandu A, Spakovsky MR, Zhao J (2019) Propagating uncertainty in power system dynamic simulations using polynomial chaos. IEEE Trans Power Syst 34(1):338–348
4. Fan M, Li Z, Ding T, Huang L, Dong F, Ren Z, Liu C (2021) Uncertainty evaluation algorithm in power system dynamic analysis with correlated renewable energy sources. IEEE Trans Power Syst 36(6):5602–5611
5. Ren J, Peng H, Jiang L, Liu Z, Wu J, Yu Z, Yu PS (2023) Uncertainty-guided boundary learning for imbalanced social event detection. IEEE Trans Knowl Data Eng 36(6):2701–2715
6. Zhang H, Li P (2011) Chance constrained programming for optimal power flow under uncertainty. IEEE Trans Power Syst 26:2417–2424
7. Guggilam SS, Dall'Anese E, Chen YC, Dhople SV, Giannakis GB (2016) Scalable optimization methods for distribution networks with high PV integration. IEEE Trans Smart Grid 7(4):2061–2070
8. Roald L, Andersson G (2017) Chance-constrained AC optimal power flow: reformulations and efficient algorithms. IEEE Trans Power Syst 33(3):2906–2918
9. Dallanese E, Baker K, Summers T (2017) Chance-constrained AC optimal power flow for distribution systems with renewables. IEEE Trans Power Systems 32(5):3427–3438
10. Venzke A, Halilbasic L, Markovic U, Hug G, Chatzivasileiadis S (2017) Convex relaxations of chance constrained AC optimal power flow. IEEE Trans Power Syst 33(3):2829–2841
11. Duan C, Fang W, Jiang L, Yao L, Liu J (2018) Distributionally robust chance-constrained approximate AC-OPF with Wasserstein metric. IEEE Trans Power Syst 33(5):4924–4936
12. Mühlpfordt T, Roald L, Hagenmeyer V, Faulwasser T, Misra S (2019) Chance-constrained ac optimal power flow: a polynomial chaos approach. IEEE Trans Power Syst 34(6):4806–4816
13. Baker K, Bernstein A (2019) Joint chance constraints in AC optimal power flow: improving bounds through learning. IEEE Trans Smart Grid 10(6):6376–6385
14. Lubin M, Dvorkin Y, Roald L (2019) Chance constraints for improving the security of ac optimal power flow. IEEE Trans Power Syst 34(3):1908–1917
15. Molzahn DK (2017) Computing the feasible spaces of optimal power flow problems. IEEE Trans Power Syst 32:4752–4763
16. Lehmann K, Grastien A, Van Hentenryck P (2016) AC-feasibility on tree networks is NP-Hard. IEEE Trans Power Syst 31:798–801
17. Bienstock D, Verma A (2019) Strong NP-hardness of AC power flows feasibility. Oper Res Lett 47:494–501
18. Zhang L, Wang X, Liu T, Zhang Y, Hu Y (2023) A novel Brownian motion-based hybrid whale optimization algorithm. J Internet Technol 24(3):795–808
19. Almodfer R, Mudhsh M, Chelloug S, Shehab M, Abualigah L, Abd Elaziz M (2022) Quantum mutation reptile search algorithm for global optimization and data clustering. Hum-centric Comput Inf Sci 12:30
20. Dong Q, Zhu F, Xia J, Lu M (2023) Latency trade-off of particle swarm optimization-enabled seamless handoff in mobile WSNs. Hum-Centric Comput Inf Sci 13:37
21. Roald LA, Pozo D, Papavasiliou A, Molzahn DK, Kazempour J, Conejo A (2023) Power systems optimization under uncertainty: a review of methods and applications. Electr Power Syst Res 214:108725
22. Cao D, Hu W, Xu X, Wu Q, Huang Q, Chen Z, Blaabjerg F (2021) Deep reinforcement learning based approach for optimal power flow of distribution networks embedded with renewable energy and storage devices. J Mod Power Syst Clean Energy 9(5):1101–1110
23. Xu Y, Gao W, Li Y (2024) Cost-effective optimization of the grid-connected residential photovoltaic battery system based on reinforcement learning. Hum-Centric Comput Inf Sci 14:02
24. Song Y, Xiao L, Wang L, Wei W, Wang J (2023) Joint online optimization of task rescheduling and data redistribution. J Internet Technol 24(1):11–22
25. Jia M, Hug G, Su Y, Shen C (2023) Chance-constrained OPF: a distributed method with confidentiality preservation. IEEE Trans Power Syst 38(4):3373–3387
26. Bienstock D, Chertkov M, Harnett S (2014) Chance-constrained optimal power flow: risk-aware network control under uncertainty. SIAM Rev 56(3):461–495
27. Jabr RA, Karaki S, Korbane JA (2015) Robust multi-period OPF with storage and renewables. IEEE Trans Power Syst 30(5):2790–2799
28. Vrakopoulou M, Li B, Mathieu JL (2017) Chance constrained reserve scheduling using uncertain controllable loads Part I: formulation and scenario-based analysis. IEEE Trans Smart Grid 10(2):1608–1617
29. Li B, Vrakopoulou M, Mathieu JL (2017) Chance constrained reserve scheduling using uncertain controllable loads Part II: analytical reformulation. IEEE Trans Smart Grid 10(2):1618–1625
30. Zhang Y, Shen S, Mathieu JL (2016) Distributionally robust chance-constrained optimal power flow with uncertain renewables and uncertain reserves provided by loads. IEEE Trans Power Syst 32(2):1378–1388
31. Xie W, Ahmed S (2017) Distributionally robust chance constrained optimal power flow with renewables: a conic reformulation. IEEE Trans Power Syst 33(2):1860–1867
32. Lubin M, Dvorkin Y, Backhaus S (2015) A robust approach to chance constrained optimal power flow with renewable generation. IEEE Trans Power Syst 31(5):3840–3849
33. Yang L, Xu Y, Gu W, Sun H (2021) Distributionally robust chance-constrained optimal power-gas flow under bidirectional interactions considering uncertain wind power. IEEE Trans Smart Grid 12:1722–1735
34. Roald L, Misra S, Krause T, Andersson G (2016) Corrective control to handle forecast uncertainty: a chance constrained optimal power flow. IEEE Trans Power Syst 32(2):1626–1637
35. Pena-Ordieres A, Molzahn DK, Roald L, Waechter A (2021) DC optimal power flow with joint chance constraints. IEEE Trans Power Syst 36(1):147–158
36. Wang J, Wang C, Liang Y, Bi T, Shafie-Khah M, Catalao JP (2021) Data-driven chance-constrained optimal gas-power flow calculation: a Bayesian nonparametric approach. IEEE Trans Power Syst 36:4683–4698
37. Yang L, Xu Y, Sun H, Wu W (2022) Tractable convex approximations for distributionally robust joint chance-constrained optimal power flow under uncertainty. IEEE Trans Power Syst 37:1927–1941
38. Lejeune MA, Dehghanian P (2020) Optimal power flow models with probabilistic guarantees: a Boolean approach. IEEE Trans Power Syst 35:4932–4935
39. Xu J, Sun Q, Mo H, Dong D (2022) Online routing for smart electricity network under hybrid uncertainty. Automatica 145:110538
40. Vrakopoulou M, Margellos K, Lygeros J, Andersson G (2013) A probabilistic framework for reserve scheduling and N - 1

security assessment of systems with high wind power penetration. IEEE Trans Power Syst 28(4):3885–3896
41. Geng X, Xie L (2019) Data-driven decision making in power systems with probabilistic guarantees: theory and applications of chance-constrained optimization. Annu Rev Control 47:341–363
42. Yang Y, Wu W, Xu S, Lin C, Wang B (2024) Allocating cost of uncertainties from renewable generation in stochastic electricity market: general mechanism and analytical solution. IEEE Trans Power Syst 39:4224–4239
43. Chen W, Sim M, Sun J, Teo C-P (2010) From CVaR to uncertainty set: implications in joint chance-constrained optimization. Oper Res 58:470–485
44. Xu Y, Korkali M, Mili L, Chen X, Min L (2019) Risk assessment of rare events in probabilistic power flow via hybrid multi-surrogate method. IEEE Trans Smart Grid 11(2):1593–1603
45. Roald L, Misra S, Krause T, Andersson G (2017) Corrective control to handle forecast uncertainty: a chance constrained optimal power flow. IEEE Trans Power Syst 32:1626–1637
46. Roald L, Andersson G (2018) Chance-constrained AC optimal power flow: reformulations and efficient algorithms. IEEE Trans Power Syst 33:2906–2918
47. Luedtke J, Ahmed S (2008) A sample approximation approach for optimization with probabilistic constraints. SIAM J Optim 19(2):674–699
48. Roald L, Oldewurtel F, Krause T, Andersson G (2013) Analytical reformulation of security constrained optimal power flow with probabilistic constraints. In: 2013 IEEE Grenoble Conference PowerTech. POWERTECH 2013:2013
49. Stott B, Jardim J, Alsaç O (2009) DC power flow revisited. IEEE Trans Power Syst 24(3):1290–1300
50. Wood AJ, Wollenberg BF, Sheblé GB (2013) Power generation, operation, and control. Wiley, New York
51. Soman SS, Zareipour H, Malik O, Mandal P (2010) A review of wind power and wind speed forecasting methods with different time horizons. In: North American Power Symposium. IEEE, pp 1–8
52. Jiang X, Dong B, Xie L, Sweeney L (2010) Adaptive Gaussian process for short-term wind speed forecasting. In: ECAI, pp 661–666
53. Rasmussen CE, Nickisch H (2010) Gaussian processes for machine learning (GPML) toolbox. J Mach Learn Res 11:3011–3015
54. Gurobi Optimization LLC (2020) Gurobi Optimizer Reference Manual
55. Luedtke J (2007) Integer programming approaches for some non-convex and stochastic optimization problems. Georgia Institute of Technology, Atlanta
56. Luedtke J, Ahmed S, Nemhauser GL (2010) An integer programming approach for linear programs with probabilistic constraints. Math Program 122(2):247–272
57. Ahmed S, Shapiro A (2008) Solving chance-constrained stochastic programs via sampling and integer programming. In: State-of-the-art decision-making tools in the information-intensive age. Informs, pp 261–269
58. Campi MC, Garatti S, Prandini M (2009) The scenario approach for systems and control design. Annu Rev Control 33(2):149–157
59. Aigner K-M, Clarner J-P, Liers F, Martin A (2022) Robust approximation of chance constrained DC optimal power flow under decision-dependent uncertainty. Eur J Oper Res 301:318–333
60. Jabr RA (2020) Distributionally robust CVaR constraints for power flow optimization. IEEE Trans Power Syst 35:3764–3773
61. Babaeinejadsarookolaee S, Birchfield A, Christie RD, Coffrin C, DeMarco C, Diao R, Ferris M, Fliscounakis S, Greene S, Huang R, Josz C, Korab R, Lesieutre B, Maeght J, Molzahn DK, Overbye TJ, Panciatici P, Park B, Snodgrass J, Zimmerman R (2019) The power grid library for benchmarking AC optimal power flow algorithms. arXiv, pp 1–17
62. Zimmerman RD, Murillo-Sánchez CE, Thomas RJ (2010) MATPOWER: steady-state operations, planning, and analysis tools for power systems research and education. IEEE Trans Power Syst 26(1):12–19
63. ApS M (2024) The MOSEK optimization toolbox for MATLAB manual. Version 10.1